Chinese Physics Letters **41**, 028101 (2024)

High-Performance Organic Field-Effect Transistors Based on Two-Dimensional Vat Orange 3 Crystals

Ning Yan(闫宁)[1,2], Zhiren Xiong(熊志仁)[1,2], Chengbing Qin(秦成兵)[2,3], and Xiaoxi Li(李小茜)[1,2*]

[1]*State Key Laboratory of Quantum Optics and Quantum Optics Devices, Institute of Opto-Electronics, Shanxi University, Taiyuan 030006, China*
[2]*Collaborative Innovation Center of Extreme Optics, Shanxi University, Taiyuan 030006, China*
[3]*State Key Laboratory of Quantum Optics and Quantum Optics Devices, Institute of Laser Spectroscopy, Shanxi University, Taiyuan 030006, China*

(Received 15 November 2023; accepted manuscript online 11 January 2024)

The exploration and research of low-cost, environmentally friendly, and sustainable organic semiconductor materials are of immense significance in various fields, including electronics, optoelectronics, and energy conversion. Unfortunately, these semiconductors have almost poor charge transport properties, which range from $\sim 10^{-4}\,\mathrm{cm^2\cdot V^{-1}\cdot s^{-1}}$ to $\sim 10^{-2}\,\mathrm{cm^2\cdot V^{-1}\cdot s^{-1}}$. Vat orange 3, as one of these organic semiconductors, has great potential due to its highly conjugated structure. We obtain high-quality multilayered Vat orange 3 crystals with two-dimensional (2D) growth on h-BN surfaces with thickness of 10–100 nm using physical vapor transport. Raman's results confirm the stability of the chemical structure of Vat orange 3 during growth. Furthermore, by leveraging the structural advantages of 2D materials, an organic field-effect transistor with a 2D vdW vertical heterostructure is further realized with h-BN encapsulation and multilayered graphene contact electrodes, resulting in an excellent transistor performance with On/Off ratio of 10^4 and high field-effect mobility of $0.14\,\mathrm{cm^2\cdot V^{-1}\cdot s^{-1}}$. Our results show the great potential of Vat orange 3 with 2D structures in future nano-electronic applications. Furthermore, we showcase an approach that integrates organic semiconductors with 2D materials, aiming to offer new insights into the study of organic semiconductors.

DOI: 10.1088/0256-307X/41/2/028101

Over the past decade, significant research focusing on the development of organic semiconductors has achieved great success,[1] and the charge carrier mobility of organic field-effect transistors (OFETs) has been reported up to $40\,\mathrm{cm^2\cdot V^{-1}\cdot s^{-1}}$.[2] Although most previous studies on OFETs have focused on the fabrication and quality improvement of OFETs,[3–6] a few of groups are devoting their efforts to research on sustainable, biodegradable, low toxicity, or even metabolizable semiconductors due to their significant and non-negligible advantages in terms of being environmentally friendly, low-cost, and their large volumes compared with the traditional organic semiconductors. This means that they can be applied in various fields, such as biosensors, disposable electronic products, and implantable electronic devices.

Unfortunately, these types of semiconductor materials are extremely rare in nature, with a relatively low field-effect mobility. Until now, the range of mobility in natural semiconductors (b-carotene,[7] indigo,[8] flavonoids,[9] and Tyrian purple,[3] etc.) and nature-inspired semiconductors (perylene diimide,[10] Vat yellow 1[11] and Vat orange 3 (Vat 3),[10,12] etc.) has ranged from $\sim 10^{-4}\,\mathrm{cm^2\cdot V^{-1}\cdot s^{-1}}$ to $\sim 10^{-2}\,\mathrm{cm^2\cdot V^{-1}\cdot s^{-1}}$. These natural and nature-inspired semiconductors all have poor charge transport properties, which limit the potential applications for organic electronic elements. Therefore, it is crucial to develop and enhance performance of such organic semiconductors.

Among most organic semiconductors, Vat 3 exhibits relatively good transport properties and surprising controllability[10] due to its highly conjugated structure, which allows favorable π–π stacking interactions between molecules, thus facilitating efficient transport of charge carriers.[13] Moreover, Vat 3, known as anthanthrone, is also appealing for use in organic solar cells (OSCs) and organic light-emitting diode (OLED) applications due to its optical properties.[14] Unfortunately, Vat 3 was often used as a precursor material for constructing field-effect transistors with different transport types[13–17] due to its limited solubility in organic solvents, thus restricting its applications in OFETs as an organic semiconductor. To date, there has been little research on the charge transport properties of Vat 3, especially the crystalline form. Although Mihai *et al.*[10,12] successfully prepared OFETs of Vat 3 by vacuum deposition, the thin film of Vat 3 tended to form severe grain boundaries during coalescence, which greatly reduced charge carrier mobility, resulting in a mobility of only $1.9\times 10^{-3}\,\mathrm{m^2\cdot V^{-1}\cdot s^{-1}}$.

Recently, it has been reported that a high-quality organic semiconductor with highly ordered and excellent electrical properties can be achieved by adsorption or epitaxial growth on h-BN.[18] Zhang *et al.*[19] realized the highly ordered single-crystalline material pentacene via epitaxy on h-BN. Kim's group[20] obtained high-quality rubrene films on h-BN via vdW epitaxy. Furthermore,

*Corresponding author. Email: xiaoxili1987@sxu.edu.cn

highly ordered organic semiconductor crystallite networks have been successfully prepared on h-BN.[21] These studies have provided evidence that epitaxial growth on h-BN is a responsible approach to obtain high-quality organic semiconductor crystals with high electrical performance.

In this work, multilayered Vat 3 crystals with 2D growth on an h-BN surface with a thickness of about 10–100 nm were achieved by physical vapor transport (PVT), and Raman testing was conducted to gain further insights into the obtained Vat 3 crystals. OFETs based on Vat 3 encapsulated by top and bottom h-BN with multilayered graphene contact were fabricated. The performance exhibits dramatic improvement by two orders of magnitude in field-effect mobility compared to OFETs based on thin-film Vat 3.[10,12]

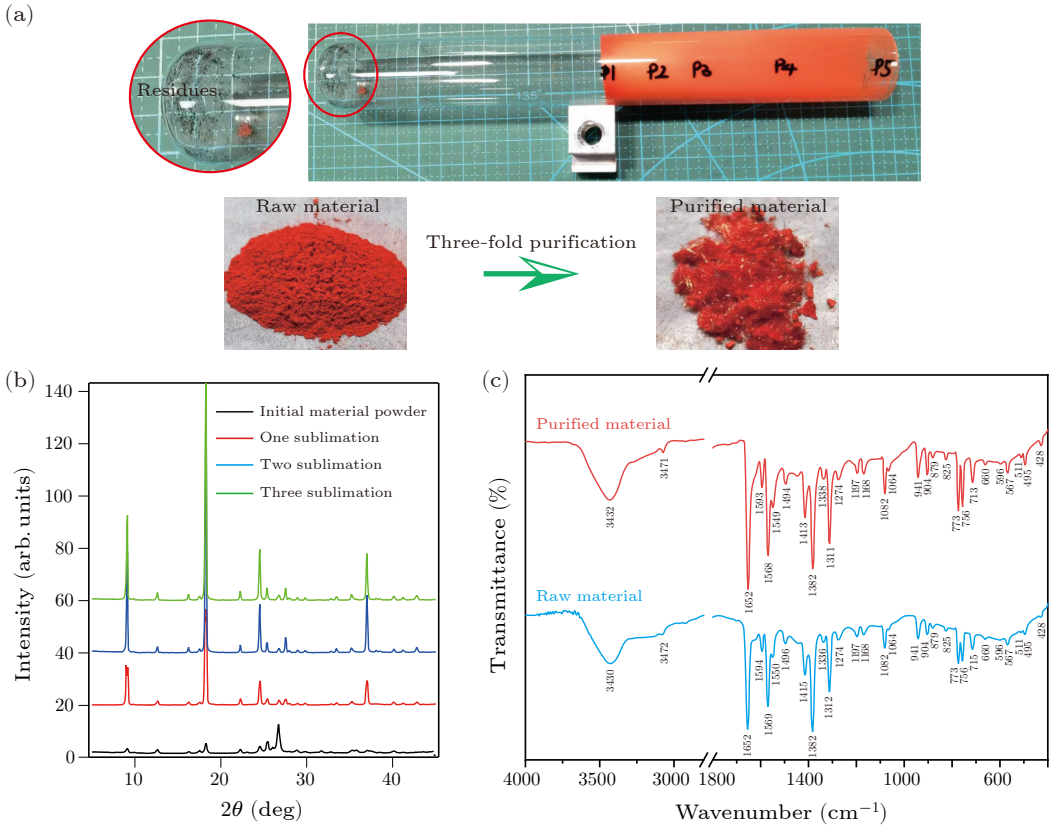

Fig. 1. Purification of Vat 3 crystals. (a) The quartz tube after the first purification step, and optical pictures of Vat 3 material before and after purification. (b) XRD spectra of materials before and after purification. (c) The infrared spectra of Vat 3 material before and after purification.

Results and Discussion. The purity of the organic semiconductor is a crucial factor in achieving high performance in OFETs. Previous studies have demonstrated that the mobility of charge carriers of OFETs can be increased by orders of magnitude by purifying the organic semiconductors.[3,22] Thus, in this work, prior to the growth process, the organic materials, Vat 3 purchased from Macklin, were purified by three cycles of vacuum sublimation in a tube furnace, similarly to Ref. [3]. As seen in Fig. 1(a), it is obvious that there was some residue left in the quartz tube after the first purification. After three purification steps, the organic material (powder) regrew into a crystalline state with an acicular shape. X-ray diffraction (XRD) measurements and infrared spectrum (IR) analysis were carried out on the raw and purified Vat 3. The results of XRD are shown in Fig. 1(b), where the degree of peaks, after regrowth, barely changes compared to the initial material powder. However, improvement in the intensity of some peaks is observed, which suggests that the crystal structure of Vat 3 has been successfully preserved during the regrowth process while enhancing in some crystal orientations. Together with the optical pictures in Fig. 1(a), it is indicated that the purification process improved the crystallinity of organic materials. Moreover, as seen in Fig. 1(c), the IR results show similar spectra before and after purifying. It is indicated that the chemical structure of Vat 3 did not undergo significant changes during the purification process, rather than introducing new chemical substances or altering the molecular structure. This further confirms that no pollution has occurred during the purifying process. With the improved high crystallinity of Vat 3, high-property field-effect transistors can be further obtained.

Subsequently, the Vat 3 crystals are grown on the surface of h-BN using the PVT method in a tube furnace, similarly to Ref. [23], as seen in the schematic diagram in Fig. 2(a). Firstly, multilayer h-BN used as the growth substrates was mechanically exfoliated and transferred onto

silicon dioxides (SiO_2), and then characterized using an optical microscope [Fig. 2(b)]. The purified Vat 3 materials are heated in the zone of the temperature detector, which is beneficial for controlling the sublimation temperature of materials accurately, then sublimed in a flow of carrier gas (high-purity argon gas here) under atmospheric pressure. The molecular vapor is carried downstream by argon gas and crystallizes in a lower temperature zone because of the temperature gradient. The benefit of this method is the combination of crystal growth with purification. In this work, the selected sublimation temperature of Vat 3 is 430 ℃, and the flow rate of argon gas is 20 ml/min. The temperature of the crystal growth zone is from 120 ℃ to 140 ℃.

Under the above conditions, Vat 3 crystals with a specific thickness were successfully obtained, as seen in the optical image in Fig. 2(c). Upon comparison with the pre-growth state [Fig. 2(b)], it is evident that the Vat 3 crystals have exhibited two distinct morphologies (acicular crystals on the surface of SiO_2, and multilayered crystals with a two-dimensional plane on h-BN), as clearly observed at the location indicated by the white arrows in Fig. 2(c). With regard to the two different morphologies of Vat 3 crystals observed in this work, this may be attributed to the competition between molecule–molecule interlayer interaction energies and molecule–substrate interaction energies during the crystal growth. When the molecule–substrate interaction energies are stronger than the interlayer interaction energies, the tendency for 2D growth is greater because of the minimum surface free energy under the 2D growth model.[24–26] Clearly, for the acicular crystals, the weak interaction energies between the molecule and SiO_2 cause crystal agglomeration with the same crystallographic orientation, which means that the crystals tend to align and grow in a needle-like shape rather than forming a flat and continuous 2D layer. Conversely, due to their stronger interaction energies between the Vat 3 molecules and h-BN, they tend to nucleate on the surface of h-BN and then undergo 2D growth, finally forming a flat and well-oriented crystal layer on h-BN, which is consistent with the results of Zhang *et al.*[19]

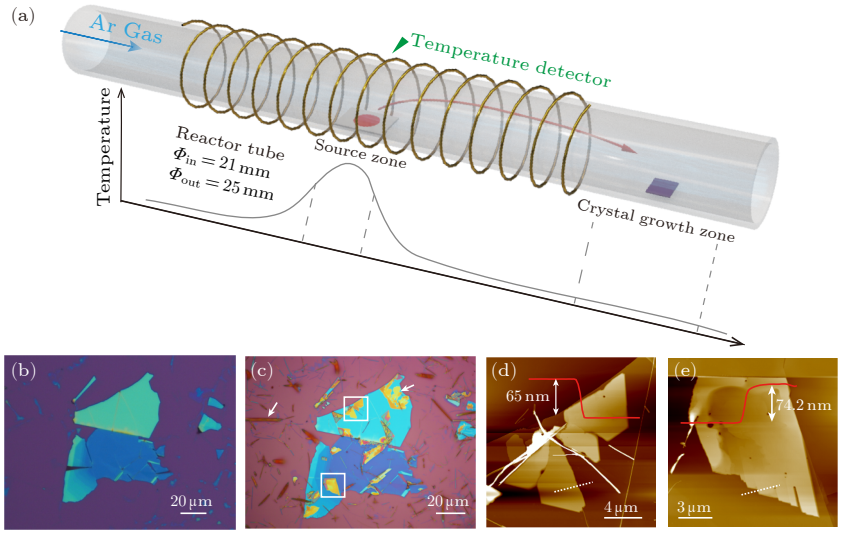

Fig. 2. Growth of Vat 3 crystals. (a) The scheme of Vat 3 crystal growth using the physical vapor transport method. [(b), (c)] Optical images of typical Vat 3 crystals on h-BN before and after crystal growth. [(d), (e)] AFM images of Vat 3 crystal on h-BN, corresponding to the white solid-line boxes in (c).

In the following discussion, we mainly focus on multilayered Vat 3 crystals grown on the surface of h-BN. This is primarily due to their favorable two-dimensional planar structures, which have relatively low energy barriers for charge injection and extraction at the interfaces within devices, and high surface-to-volume ratios for improving the efficiency and performance of devices. These properties make the multilayered Vat 3 crystals well-suited to various applications, including OFETs and logic devices. Figures 2(d) and 2(e) show the atomic force microscope (AFM) scanned images of typical Vat 3 crystals, corresponding to the white solid-line boxes shown in Fig. 2(c). The surface of Vat 3 crystals obtained by PVT is quite clean and flat, and the thickness of crystals on h-BN was about 60–70 nm. This characterization highlights the high quality and uniformity of the Vat 3 crystals, indicating their suitability for further studies and potential applications.

Furthermore, Raman spectroscopy was employed to confirm the presence of Vat 3 crystals. To exclude the influence of substrate, an additional sample consisting solely of h-BN on SiO_2 was also evaluated. By comparing the Raman spectra of pristine h-BN and Vat 3 grown on h-BN, the Raman spectrum of Vat 3 can be isolated and distinguished. It can be clearly seen that Vat 3 grown on h-BN exhibits similar features to purified Vat 3 crystals, as seen in Fig. 3(a), suggesting that Vat 3 possesses identical chemical structures and similar crystal structures. This indicates that the organic molecular structure of Vat 3 remains relatively stable during the growth process.[27] Furthermore, it is worth noting that despite the similar

Raman spectra between Vat 3 crystals before and after growth, there may still be some deviations in the individual Raman peaks. However, we could not understand the exact cause of these deviations based only on the Raman results. The potential reasons for these deviations may be the differences in lattice or lattice defects introduced during the growth process, which require further investigation and development.

Figures 3(b)–3(d) show the photoluminescence (PL) spectra of multilayered Vat 3 crystals on h-BN with angle-resolved excitation and emission polarization using a 532 nm laser. The PL of multilayered Vat 3 exhibits two non-negligible peaks at 2.01 eV and 2.12 eV, respectively, as seen in Fig. 3(b). The energy difference of the value 0.11 eV between the two peaks can be primarily attributed to the energy-level transitions within the Vat 3 molecule.[28] By extracting the peak values from the PL curves at different emission polarization angles (θ) ranging from 0° to 360°, a strong dependence relationship with a periodicity of 180° can be observed at room temperature. Here, the dichroic ratio (DR) is expressed as the ratio of the highest PL peak intensity values to the lowest, which is extracted at 0° and 90° in our measurements, respectively. As shown in Figs. 3(c) and 3(d), the DR value in the Vat 3 sample reaches up to 9.36, comparable to the reported results in organic semiconductor materials.[19,29] This indicates that the emission of multilayered Vat 3 exhibits significant polarization characteristics in different directions, suggesting the presence of strong in-plane anisotropy.

Next, we focus on electrical properties of multilayered Vat 3 grown on h-BN. Firstly, conventional direct contacts were selected to fabricate the devices, as seen in the typical optical image in the inset image of Fig. 4(a). Source-drain Au electrodes (100 nm) were fabricated by electron-beam evaporation using photoresist and electron-beam lithography technology. Highly conductive silicon was used as a global back-gate. Figures 4(a) and 4(b) show the room-temperature output and transfer characteristics of the multilayered Vat 3 OFET. Under a bias voltage of 10 V, the on-current achieved is 500 nA with a 10^6 on/off ratio. Additionally, the carrier mobility of the multilayered Vat 3 crystal as a function of V_{gs} is calculated [see Fig. 4(c)] and extruded using the following equation:

$$\mu = \frac{dI_{ds}}{dV_{gs}} \frac{L}{W} \frac{1}{C_{bg} V_{ds}}, \tag{1}$$

$$C_{bg} = \frac{\varepsilon_0}{d_1/\varepsilon_1 + d_2/\varepsilon_2}, \tag{2}$$

where μ represents the field-effect mobility, I_{ds} and V_{gs} are the source-drain current and gate voltage, W and L are the geometric factors of the channel (length and width), C_{bg} is the specific capacitance of the bottom dielectric, and d_1 and d_2 are the thicknesses of the h-BN (∼30 nm) dielectric and SiO_2 (∼285 nm) dielectric, respectively. All of the mobilities in this study are extracted from the linear regime.

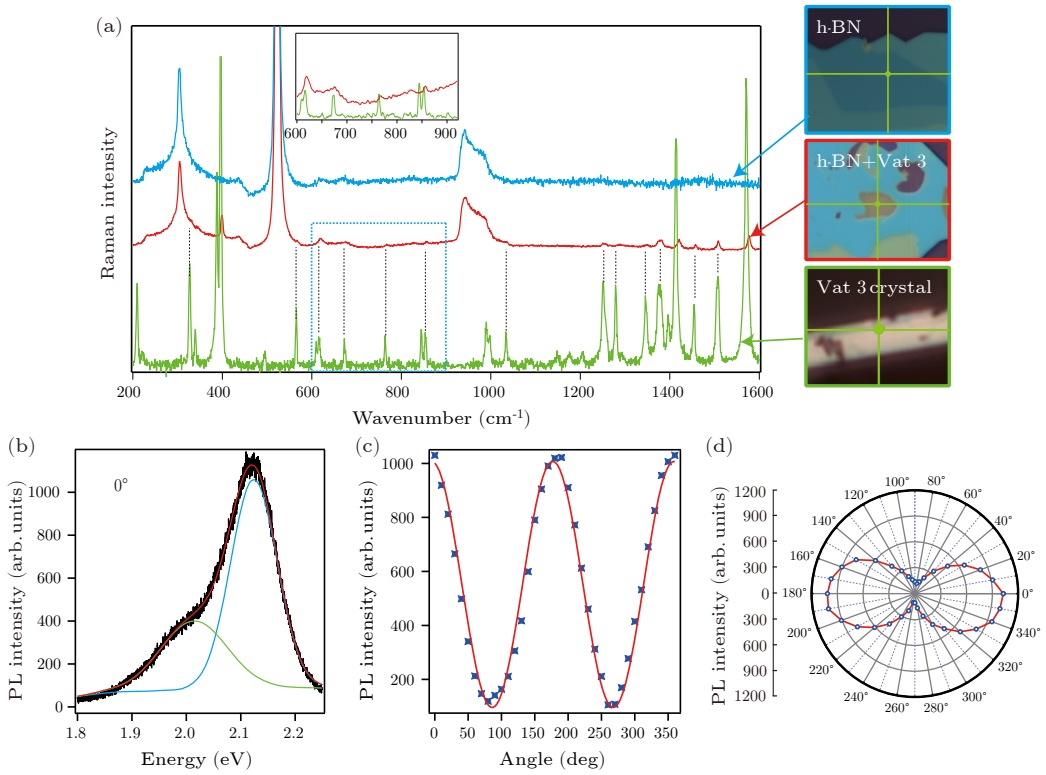

Fig. 3. Crystal characterization of multilayered Vat 3 on h-BN. (a) The Raman spectrum of h-BN (blue line), Vat 3 on h-BN (red line), and Vat 3 crystal (green line), respectively, using a 785 nm laser. (b)–(d) Photoluminescence spectra of multilayered Vat 3 crystals on h-BN with angle-resolved excitation and emission polarization using a 532 nm laser.

As seen in Fig. 4(c), the field-effect mobilities under bias voltages of 5 V and 10 V exhibit distinct behavior with peak mobilities of ~ 0.02 and $\sim 0.03\,\mathrm{cm^2{\cdot}V^{-1}{\cdot}s^{-1}}$, respectively. Compared with the carrier mobility of vacuum-processed Vat 3 thin-film transistors,[10,12] our results represent a slight improvement by one order of magnitude. The higher carrier mobility observed in our results suggests that the molecular stacking arrangement in multilayered Vat 3 crystals on h-BN is more favorable for electron migration, in which conjugated molecules have strong interactions with neighboring molecules to maximize the overlap of π molecular orbits. Moreover, the thin films that undergo three-dimensional growth at the dielectric interface tend to form severe grain boundaries during the coalescence process. These grain boundaries act as trap sites and significantly reduce the mobility of charge carriers.[30]

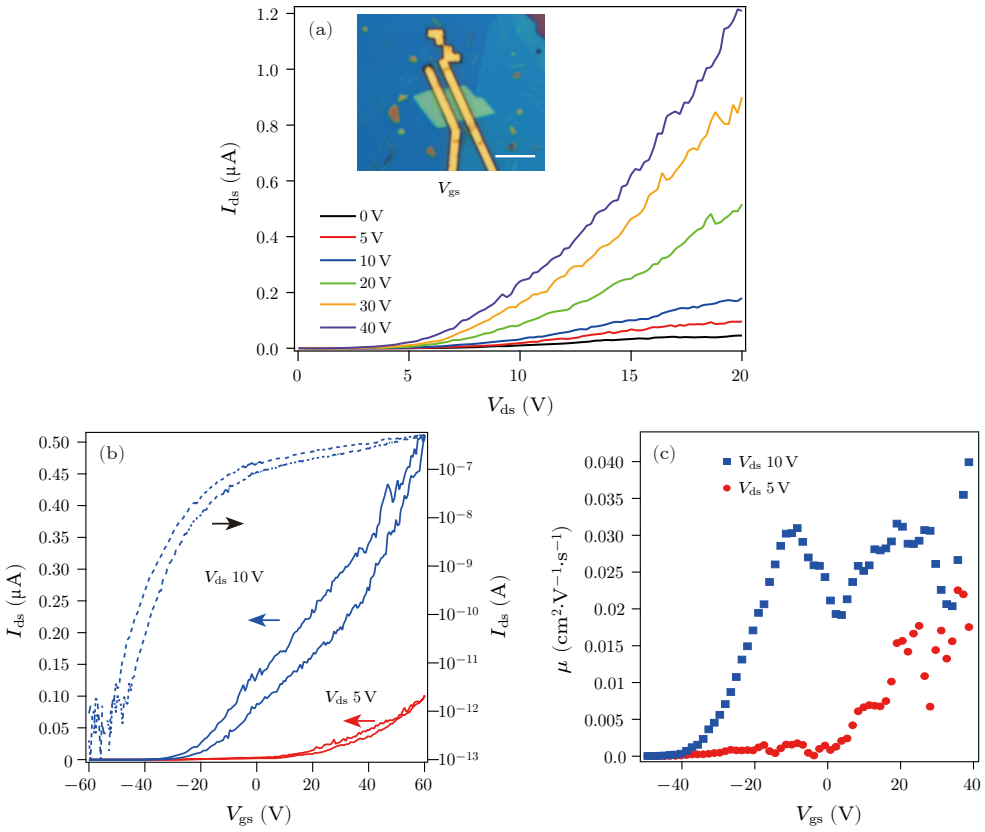

Fig. 4. Electrical properties of multilayered Vat 3 grown on h-BN with conventional direct contacts. (a) I–V curves along various gate voltages from 0 V to 40 V. Inset: an optical image of a typical Vat 3 device; the scale bar: 10 μm. (b) Transfer curves of devices with different source-drain voltages. The dashed blue line is the same data as the solid blue line in a semilog plot. (c) The extracted carrier mobility at $V_{ds} = 5$ V and 10 V.

Regrettably, despite the slight improvement in the field-effect mobility, it remains extremely limited, and the data with conventional direct contacts appears to be very unstable. This could be attributed to unreasonable operating procedures during the device fabrication process. It has been reported that organic semiconductor crystals, in contrast to traditional semiconductor materials, are easily polluted by organic solvent (photoresist, acetone, etc) during fabrication or are damaged by the thermal irradiation during the vacuum deposition of electrodes, resulting in poor performance of OFETs.[31] Moreover, the I–V results [Fig. 4(a)] suggest that there is a considerable contact resistance between the Au source/drain electrodes and multilayered Vat 3 crystal, which is one of the non-negligible factors that may contribute to the observed low mobility.

To further enhance the performance of our devices, we have redesigned and optimized the structure of the OFET, leveraging the advantages of 2D materials. As seen in Fig. 5(a), a multilayered h-BN was used as a top layer to encapsulate multilayered Vat 3 crystal and to provide protection from direct exposure to potential dangers.[32,33] Multilayered graphene, as an excellent conductor with a relatively low work function (about 4.3 eV), was used as the electrode material to interface with the multilayered Vat 3 crystal to match the lowest unoccupied molecular orbital of Vat 3, about $\sim$ 3.8 eV.[11,34] In addition, highly conductive silicon was used as a global back-gate similarly. After fabrication of the heterostructure using the dry transfer method, further processing of the multilayered graphene contact 2D heterostructure OFET in the form of h-BN/multilayered graphene/Vat 3 crystal/h-BN was carried out using standard micro–nano processing technology, including electron beam lithography, reactive ion etching and electron beam evaporation.

Obviously, higher transistor performance is obtained in OFETs with 2D heterostructures, as seen in Figs. 5(b)–

5(d). Under the protection of the top-layer h-BN and the connection of multilayered graphene electrodes [inset image in Fig. 5(b)], the maximum on-current can reach 300 nA with a bias voltage as low as 2 V with a 10^4 on/off ratio at $V_{bg} = 60$ V, as seen in the I–V and transfer curves in Figs. 5(b) and 5(c); meanwhile, the maximum of the source-drain current in our device is on the microampere scale. Furthermore, the field-effect mobility has also significantly increased with the redesigned and optimized OFET structure using graphene electrodes. The peak mobilities under bias voltages of 1 V and 2 V are $\sim$0.1 and $\sim$0.14 $cm^2 \cdot V^{-1} \cdot s^{-1}$ [Fig. 5(d)], respectively, which have increased by one order of magnitude compared to the OFET with conventional direct contacts, and by two orders of magnitude compared to vacuum-processed Vat 3 thin-film transistors.[10,12] Compared with other similar semiconductors, such as Vat orange 9 (1.4×10^{-4} $cm^2 \cdot V^{-1} \cdot s^{-1}$ [35]), Vat yellow 4 (1.5×10^{-4} $cm^2 \cdot V^{-1} \cdot s^{-1}$ [35]), indigo (2×10^{-4} $cm^2 \cdot V^{-1} \cdot s^{-1}$ [8]), Vat yellow 1 (0.012 $cm^2 \cdot V^{-1} \cdot s^{-1}$ [11]), and Vat blue 4 (7.5×10^{-3} $cm^2 \cdot V^{-1} \cdot s^{-1}$ [36]), the performance of the Vat 3 reported here has great advantages in OFETs. Moreover, the optimized device exhibits a more linear I–V curve. This indicates that using graphene as electrodes has successfully reduced the electronic injection barrier, which may be one of the main reasons why the optimized device demonstrates high transistor performance. Another significant reason is that the optimized OFET structure effectively protects the Vat 3 crystal, preventing damage during the device fabrication process.

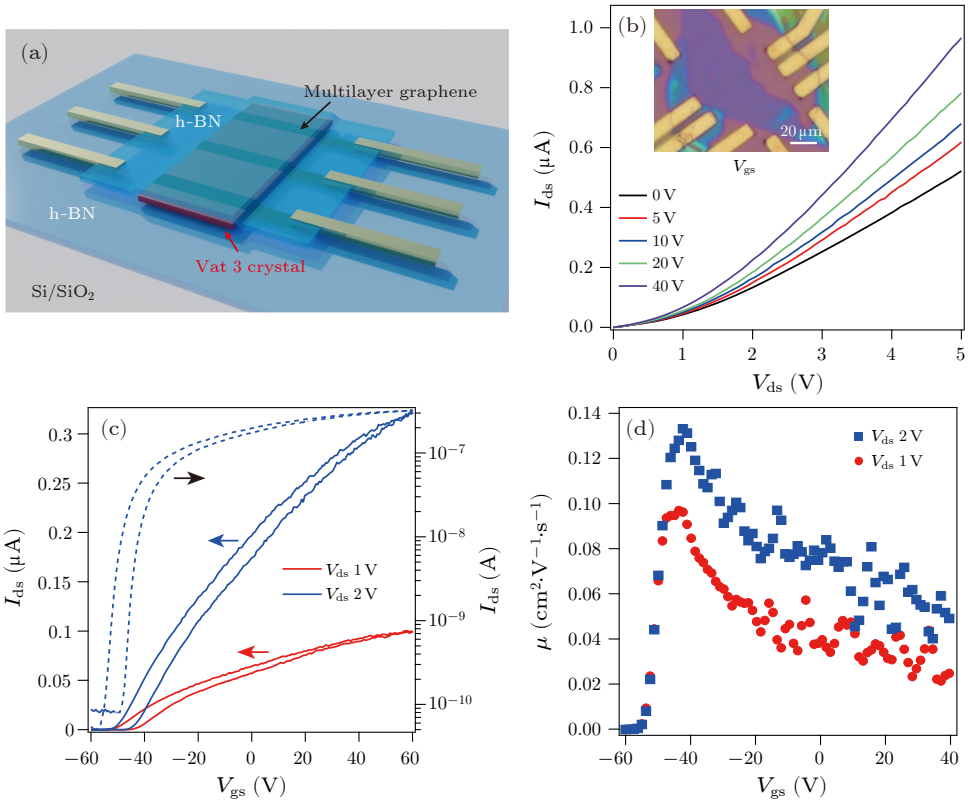

Fig. 5. Electrical properties of multilayered Vat 3 grown on h-BN with multilayered graphene contacts. (a) A scheme of the device structure. (b) Room-temperature I_{ds}–V_{ds} characteristics of the device under different V_{gs}. The inset is the optical image of a typical device. (c) Room-temperature transfer characteristics of the device. (d) The calculated field-effect mobility as a function of V_{gs}.

In summary, we have successfully fabricated OFETs based on the low-cost, environmentally friendly, and sustainable organic semiconductor Vat 3. Using the PVT method, multilayered Vat 3 crystals with 2D morphology were successfully obtained on the surface of h-BN. The Raman and PL spectra further demonstrated the high quality of the Vat 3 crystals. Through h-BN encapsulation and graphene contact, the carrier mobility of the high-quality OFET based on the multilayered Vat 3 heterostructure can reach up to 0.14 $cm^2 \cdot V^{-1} \cdot s^{-1}$, which is significantly improved compared to the OFETs of Vat 3 with direct contacts. Our results offer new insights into the study of organic semiconductors and pave the way for the future development of vertical assemblies based on organic semiconductors.

Method. In this work, AFM and Raman measurements were carried out using a Bruker Icon system and a HORIBA (LabRAM Odyssey), respectively. A laser with 785 nm wavelength and 2 mW power was applied in this study. The infrared spectra (wave number range of 400–4000 cm^{-1}) were recorded on a Fourier transform infrared spectrometer (BRUKER TENSOR) by mixing the samples with KBr pellets and pressing into plates for tests. For the Vat 3 heterostructure with graphene electrodes, top-layer

h-BN and multilayered graphene were stacked in sequence using a dry transfer procedure,[37] then deposited onto the surface of Vat 3 at 120 ℃ and cleaned with acetone to complete the preparation of the heterostructure. Au electrodes with thickness of 100 nm were deposited onto the surface of Vat 3 or contact graphene using standard micro–nano processing technology: specifically, electron beam lithography, reactive ion etching, and electron beam evaporation, to form conventional direct contacts and graphene contacts, respectively. Electrical measurements were performed using a Keithley 1500A semiconductor parameter analyzer under an atmospheric environment.

Acknowledgement. This work was supported by the National Natural Science Foundation of China (Grant Nos. U21A6004, 62375160, 62274180, and 12004389).

References

[1] Paterson A F, Singh S, Fallon K J, Hodsden T, Han Y, Schroeder B C, Bronstein H, Heeney M, McCulloch I, and Anthopoulos T D 2018 *Adv. Mater.* **30** 1801079
[2] Kwon S, Kim J, Kim G, Yu K, Jo Y R, Kim B J, Kim J, Kang H, Park B, and Lee K 2015 *Adv. Mater.* **27** 6870
[3] Yumusak C, Sariciftci N S, and Irimia-Vladu M 2020 *Mater. Chem. Front.* **4** 3678
[4] Pfattner R, Mas-Torrent M, Bilotti I, Brillante A, Milita S, Liscio F, Biscarini F, Marszalek T, Ulanski J, Nosal A, Gazicki-Lipman M, Leufgen M, Schmidt G, Molenkamp L W, Laukhin V, Veciana J, and Rovira C 2010 *Adv. Mater.* **22** 4198
[5] Chen M, Peng B Y, Sporea R A, Podzorov V, and Chan P K L 2022 *Small Sci.* **2** 2100115
[6] Chen Y, Yan C, Dong J, Zhou W, Rosei F, Feng Y, and Wang L N 2021 *Adv. Funct. Mater.* **31** 2104099
[7] Burch R R, Dong Y H, Fincher C, Goldfinger M, and Rouviere P E 2004 *Synth. Met.* **146** 43
[8] Irimia-Vladu M, Głowacki E D, Troshin P A, Schwabegger G, Leonat L, Susarova D K, Krystal O, Ullah M, Kanbur Y, and Bodea M A 2012 *Adv. Mater.* **24** 375
[9] Hou C Y and Chen X 2015 *Mol. Phys.* **113** 521
[10] Irimia-Vladu M, Troshin P A, Reisinger M, Shmygleva L, Kanbur Y, Schwabegger G, Bodea M, Schwödiauer R, Mumyatov A, Fergus J W, Razumov V F, Sitter H, Sariciftci N S, and Bauer S 2010 *Adv. Funct. Mater.* **20** 4069
[11] Glowacki E D, Leonat L, Voss G, Bodea M, Bozkurt Z, Irimia-Vladu M, Bauer S, and Sariciftci N S 2011 *Proc. SPIE* **8118** 81180M
[12] Irimia-Vladu M, Troshin P A, Reisinger M, Schwabegger G, Ullah M, Schwoediauer R, Mumyatov A, Bodea M, Fergus J W, and Razumov V F 2010 *Org. Electron.* **11** 1974
[13] Giguère J B, Verolet Q, and Morin J F 2013 *Chem. - Eur. J.* **19** 372
[14] Morin J F 2017 *J. Mater. Chem. C* **5** 12298
[15] Giguère J B, Sariciftci N S, and Morin J F 22015 *J. Mater. Chem. C* **3** 601
[16] Liu Q, Wang Y, Arunagiri L, Khatib M, Manzhos S, Feron K, Bottle S E, Haick H, Yan H, Michinobu T, and Sonar P 2020 *Mater. Adv.* **1** 3428
[17] Chen L, Xing F, Lin Q, Waqas A, Wang X, Baumgartner T, and He X 2023 *Batteries Supercaps* **6** e202200406
[18] Kratzer M, Matkovic A, and Teichert C 2019 *J. Phys. D* **52** 383001
[19] Zhang Y H, Qiao J S, Gao S, Hu F R, He D W, Wu B, Yang Z Y, Xu B C, Li Y, Shi Y, Ji W, Wang P, Wang X, Xiao M, Xu H, Xu J B, and Wang X 2016 *Phys. Rev. Lett.* **116** 016602
[20] Lee C H, Schiros T, Santos E J, Kim B, Yager K G, Kang S J, Lee S, Yu J, Watanabe K, and Taniguchi T 2014 *Adv. Mater.* **26** 2812
[21] Matković A, Genser J, Lüftner D, Kratzer M, Gajić R, Puschnig P, and Teichert C 2016 *Sci. Rep.* **6** 38519
[22] Reese C and Bao Z 2007 *Mater. Today* **10** 20
[23] Jiang H and Kloc C 2013 *MRS Bull.* **38** 28
[24] Virkar A A, Mannsfeld S, Bao Z, and Stingelin N 2010 *Adv. Mater.* **22** 3857
[25] Markov I 2003 *Growth and Epitaxy* (Singapore: World Scientific)
[26] Li R J, Zhang X T, Dong H L, Li Q K, Shuai Z G, and Hu W P 2016 *Adv. Mater.* **28** 1697
[27] Fernandes J D, Macedo W C, Vieira D H, Furini L N, and Alves N 2023 *Thin Solid Films* **772** 139808
[28] Xu X, Qiao J, Sun B, Tao L, Zhao Y, Qin M, Lu X, Ji W, Chen Z, and Xu J 2020 *ACS Appl. Electron. Mater.* **2** 2888
[29] Sharma A, Zhang L, Tollerud J O, Dong M, Zhu Y, Halbich R, Vogl T, Liang K, Nguyen H T, and Wang F 2020 *Light: Sci. & Appl.* **9** 116
[30] Ito Y, Virkar A A, Mannsfeld S, Oh J H, Toney M, Locklin J, and Bao Z 2009 *J. Am. Chem. Soc.* **131** 9396
[31] Li R J, Hu W P, Liu Y Q, and Zhu D B 2010 *Acc. Chem. Res.* **43** 529
[32] Wang H W, Chen M L, Zhu M J, Wang Y N, Dong B J, Sun X D, Zhang X R, Cao S, Li X X, and Huang J Q 2019 *Nat. Commun.* **10** 2302
[33] Shao Y J, Zhou J, Xu N, Chen J, Watanabe K, Taniguchi T, Shi Y, and Li S L 2023 *Chin. Phys. Lett.* **40** 068501
[34] Leonat L, Sbarcea G, and Branzoi I V 2013 *UPB Sci. Bull. Ser. B* **75** 111
[35] Chetyrkina M R, Talalaev F S, Kameneva L V, Kostyuk S V, and Troshin P A 2022 *J. Mater. Chem. C* **10** 3224
[36] Irimia-Vladu M, Kanbur Y, Camaioni F, Coppola M E, Yumusak C, Irimia C V, Vlad A, Operamolla A, Farinola G M, and Suranna G P 2019 *Chem. Mater.* **31** 6315
[37] Wang L, Meric I, Huang P Y, Gao Q, Gao Y, Tran H, Taniguchi T, Watanabe K, Campos L, Muller D, Guo J, Kim P, Hone J, Shepard K L, and Dean C R 2013 *Science* **342** 614